

Thermodynamic and topological properties of copolymer rings with a segregation/mixing transition

E J Janse van Rensburg¹, E Orlandini², M C Tesi³ and S G Whittington⁴

¹ Department of Mathematics and Statistics, York University,
Toronto, Ontario M3J 1P3, Canada

² Dipartimento di Fisica e Astronomia e Sezione INFN, Università di Padova,
Via Marzolo 8, I-35131 Padova, Italy

³ Dipartimento di Matematica, Università di Bologna,
Piazza di Porta San Donato 5, I-40126 Bologna, Italy

⁴ Department of Chemistry, University of Toronto, Toronto M5S 3H6, Canada

July 1, 2022

Abstract

Two ring polymers close to each other in space may be either in a segregated phase if there is a strong repulsion between monomers in the polymers, or intermingle in a mixed phase if there is a strong attractive force between the monomers. These phases are separated by a critical point which has a θ -point character. The metric and topological properties of the ring polymers depend on the phase, and may change abruptly at the critical point. In this paper we examine the thermodynamics and linking of two ring polymers close in space in both the segregated and mixed phases using a cubic lattice model of two polygons interacting with each other. Our results show that the probability of linking is low in the segregated phase, but that it increases through the critical point as the model is taken into the mixed phase. We also examine the metric and thermodynamic properties of the model, with focus on how the averaged measures of topological complexity are related to these properties.

Keywords: Links, lattice polygons, polymer collapse, Monte Carlo methods.

1 Introduction

Mutually attracting pairs of circular or ring polymers in solution undergo a transition from a segregated to a mixed phase at a critical temperature. The metric and topological properties of the polymers are different in the segregated and mixed phases, changing at the critical temperature from expanded spatially segregated conformations to more compact conformations in the mixed phase where the two polymers interpenetrate. In [1] the segregation-mixing transition of a polymer-polymer-solvent mixture is discussed in chapter IV.4. There it is argued that in a good solvent the polymer coils behave like hard spheres which cannot interpenetrate (they are segregated). In a poor solvent, however, the coils tend to exclude the solvent and are driven together increasing the local concentration which, if high enough, should drive the system through a θ -transition into

a collapsed phase. This should also occur if there is a strong attractive interaction between the polymer coils, where they exclude solvent molecules by mixing in close proximity to one another.

In this paper we aim to model the segregated-mixed phases in a model of a system composed of a pair of proximate ring polymers which may be linked, especially when they are in the mixed phase. We use a cubic lattice closed self-avoiding walk model (lattice polygons) where the proximity is modelled by forcing the polygons to have at least one pair of vertices (one vertex in each polygon) a unit distance apart. See figure 1(a) for an example. The two polygons are both self-avoiding and mutually avoiding in the lattice.

Our model is also useful as a model for a particular class of diblock copolymers with figure eight connectivity composed of two polygons joined together by sharing a single step (see figure 1b). Each polygon is a block in the copolymer, and both polygons are in a good solvent but there is a short range interaction *between* vertices located in each of the two polygons. If the interaction is a strong attractive force, then the two polygons in the figure eight will tend to interpenetrate, otherwise they will segregate due to an entropic repulsion between them. One may also consider ring formation in a uniform 4-star polymer with two *A*-arms and two *B*-arms. The star polymer can be cyclized to form an *A* ring and a *B* ring, in conditions with different interaction strengths between the two rings, resulting in different extents of linking of the two rings.

We shall focus (in particular) on the metric and topological properties of our model in the segregated and mixed phases. Our aim is to address the following questions:

- How do configurational properties (such as mean extension, shape and entanglement) depend on the strength of the interaction between the component polygons (or blocks)?
- How do topological properties of the system (such as the complexity of linking between the component polygons) differ in the segregated and mixed phases?
- How does topological complexity, as measured in terms of the link spectrum, depend on the degree of mixing?

The configurational and topological properties of the model could be different in the segregated and mixed phases. In the segregated phase the component polygons tend to be separated in space, and so the degree of linking between them will be low, while in the mixed phase they may be strongly intermingled with a high degree of linking. It is not clear *a priori* that the transition will be strongly signalled in the configurational properties of the model. While the segregated phase will have the scaling properties of a self-avoiding walk, as the model crosses the critical point into the mixed phase the two polygons might form ribbon-like structures [2, 3]. If this is all that happens then the critical exponents of the mixed phase will still be given by self-avoiding walk exponents. The interactions between different parts of the ribbon boundaries could lead to further collapse, similar to that of a self-avoiding walk having gone through a θ -transition into its dense phase. This transition should be signalled in the linking (and in the mean topological invariants such as linking number) of the two components, and the critical properties (such as the radius of gyration exponent) might be different on the two sides of the transition.

The plan of the paper is as follows. In section 2 we describe the model and its partition function and free energy. Section 3 contains some theorems establishing the existence of a transition from a segregated phase to a mixed phase. In section 4 we discuss the Monte Carlo methods used to sample configurations and consider the results of the simulations (and in particular the metric and shape properties of the system as a function of the attractive interaction). Results on the topological

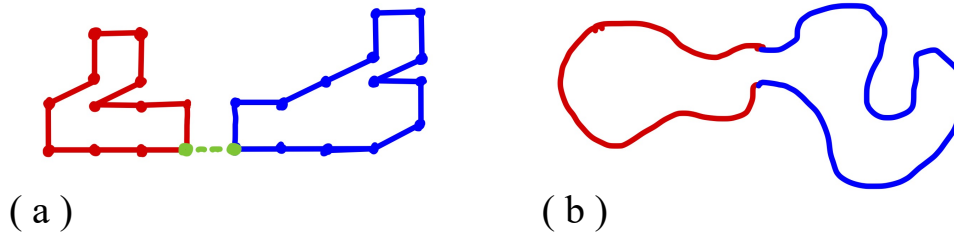


Figure 1: (a) The model. The dashed line joining a vertex in each component is rooted (that is, it cannot be moved by an elementary move in the Monte Carlo algorithm). (b) A diblock copolymer ring with the ends of the two blocks forced to be nearest neighbours in space. This approximates a figure eight conformation with each polygon ring a block in the copolymer.

mutual entanglement are presented and discussed in section 5. We close with a short Discussion in section 6.

2 The model

We model circular polymers as lattice self-avoiding polygons of length n . These are embeddings of simple closed curves in the simple cubic lattice \mathbb{Z}^3 . The embeddings are also simple closed curves in \mathbb{R}^3 with well defined topological properties (knots and links). In this paper the lattice polygons are mutually avoiding and placed in \mathbb{Z}^3 such that a pair of vertices (one vertex in each polygon) are a unit distance apart (see figure 1). We label the two polygons by A and B respectively so that this is a model of two adjacent rings A and B which may be linked, or parts of a copolymer with a figure eight connectivity and two blocks, each a ring of the figure eight.

A *mutual contact* between polygons A and B is a pair of vertices (v_A, v_B) , such that $v_A \in A$ and $v_B \in B$ and the distance between v_A and v_B is equal to one: $d(v_A, v_B) = 1$. An interaction between the two polygons (or blocks in the copolymer) is introduced by introducing an energy ϵ_m associated with each mutual contact, and then defining the parameter $\beta_m = -\epsilon_m/k_B T$ where k_B is Boltzmann's constant and T is the absolute temperature. Denoting the number of conformations of the lattice model of total length $2n$ (each polygon component of length n) with k_m mutual contacts by $p_{2n}^{(2)}(k_m)$, the equilibrium properties of the system are given by the partition function

$$Z_{2n}(\beta_m) = \sum_{k_m} p_{2n}^{(2)}(k_m) e^{\beta_m k_m}. \quad (1)$$

Entropy dominates the model when $\beta_m \leq 0$ and the two component polygons tend to stay separated (this is a *segregated phase* due to the mutual avoidance between the polygons inducing a short-ranged repulsion between them). When $\beta_m > 0$ is large enough, then the mutual contacts induce an attraction between the component polygons, and one expects this to increase the number of mutual contacts. In this case one expects the most likely conformations to be those where the two polygons interpenetrate strongly in a *mixed phase*.

The free energy per unit length is given by $f_{2n}(\beta_m) = \frac{1}{2n} \log Z_{2n}(\beta_m)$ and by taking $n \rightarrow \infty$ the

limiting free energy of the model is obtained:

$$f(\beta_m) = \lim_{n \rightarrow \infty} \frac{1}{2n} \log Z_{2n}(\beta_m). \quad (2)$$

It is not known that this limit exists for all values of $\beta_m \in \mathbb{R}$ but we shall show that it exists for $-\infty < \beta_m \leq 0$ and is equal to $\kappa_3 = \log \mu_3$ where κ_3 is the connective constant and μ_3 is the growth constant of cubic lattice self-avoiding walks [4] (see section 3). When $\beta_m > 0$ the situation is more complicated and we shall rely on Monte Carlo simulations to explore the model in this regime.

3 Some rigorous results

In this section we obtain some bounds on the partition function $Z_{2n}(\beta_m)$ and use these to prove the existence of the thermodynamic limit when $\beta_m \leq 0$ and the existence of a phase transition in the system. We also obtain some similar results for fixed link type.

Attach the coordinate system (x_1, x_2, x_3) to \mathbb{Z}^3 so that the coordinates of the vertices are all integers. Write p_n for the number of n -edge polygons (modulo translation) so that $p_{2m+1} = 0$, $p_4 = 3$, $p_6 = 22$, etc. Hammersley [4] has shown that $\lim_{n \rightarrow \infty} \frac{1}{n} \log p_n = \log \mu_3$ where μ_3 is the growth constant of self-avoiding walks on this lattice. Similarly, if we write q_n for the corresponding number of polygons on the square lattice \mathbb{Z}^2 then $\lim_{n \rightarrow \infty} \frac{1}{n} \log q_n = \log \mu_2$ where μ_2 is the growth constant of self-avoiding walks on the square lattice.

Theorem 1. *If $-\infty < \beta_m \leq 0$ then $\lim_{n \rightarrow \infty} \frac{1}{2n} \log Z_{2n}(\beta_m) = \kappa_3 = \log \mu_3$.*

Proof: To obtain an upper bound consider $\beta_m = 0$. Embed a polygon with n edges in p_n ways and embed a second n -edge polygon in a box of side $2n$ centred on the first polygon, This implies that $Z_{2n}(0) \leq p_n^2 e^{o(n)}$ so that

$$\limsup_{n \rightarrow \infty} \frac{1}{2n} \log Z_{2n}(\beta_m) \leq \limsup_{n \rightarrow \infty} \frac{1}{2n} \log Z_{2n}(0) \leq \log \mu_3, \quad \text{if } \beta_m \leq 0.$$

To get a lower bound construct two polygons, one (σ_1) with $n-2$ edges and the other (σ_2) with n edges. For σ_1 translate the right-most top-most edge a unit distance to the right and add two edges to reconnect the polygon to form σ_3 . Translate σ_3 , and rotate it if necessary, so that its right-most edge is unit distance from an edge of σ_2 and there are exactly two vertices of σ_3 that are unit distance from vertices of σ_2 . This gives the bound

$$Z_{2n}(\beta_m) \geq p_n p_{n-2} e^{2\beta_m} / 2$$

since exactly two new mutual contacts are created. Taking logarithms, dividing by $2n$ and letting $n \rightarrow \infty$ gives

$$\liminf_{n \rightarrow \infty} \frac{1}{2n} \log Z_{2n}(\beta_m) \geq \log \mu_3$$

which completes the proof. \square

Theorem 2. *If $\beta_m > 0$ and $0 < \alpha < 1$ then*

$$\liminf_{n \rightarrow \infty} \frac{1}{2n} \log Z_{2n}(\beta_m) \geq \frac{\alpha}{2} [\log \mu_2 + \beta_m] + (1 - \alpha) \log \mu_3.$$

Since $\alpha \in (0, 1)$ is arbitrary, this shows that

$$\liminf_{n \rightarrow \infty} \frac{1}{2n} \log Z_{2n}(\beta_m) \geq \max \left(\frac{1}{2} [\log \mu_2 + \beta_m], \log \mu_3 \right).$$

Proof: Construct a polygon σ_1 in the plane $x_1 = 0$ with $[\alpha n]$ edges, $0 < \alpha < 1$. Let σ_2 be a translate of σ_1 in the plane $x_1 = 1$. Let σ_3 be a polygon in \mathbb{Z}^3 with $n - [\alpha n]$ edges and with no vertices with $x_1 > -1$. Similarly, let σ_4 be a polygon in \mathbb{Z}^3 with $n - [\alpha n]$ edges and with no vertices with $x_1 < 2$. Concatenate σ_1 and σ_3 to obtain a polygon with n edges and, similarly, concatenate σ_2 and σ_4 . The two resulting polygons have $[\alpha n]$ pairs of vertices unit distance apart so that they contribute a Boltzmann factor $\exp[\beta_m [\alpha n]]$ to the partition function $Z_{2n}(\beta_m)$. σ_1 can be chosen in $\mu_2^{[\alpha n] + o(n)}$ ways, σ_2 can be chosen in only one way, while σ_3 and σ_4 can each be chosen in $\mu_3^{n - [\alpha n] + o(n)}$ ways. This construction gives a lower bound on $Z_{2n}(\beta_m)$

$$Z_{2n}(\beta_m) \geq q_{[\alpha n]} p_{n - [\alpha n]}^2 e^{\beta_m [\alpha n]} / 4 = \mu_2^{[\alpha n] + o(n)} \mu_3^{2(n - [\alpha n]) + o(n)} e^{\beta_m [\alpha n]}.$$

Taking logarithms of the above, dividing by $2n$, and letting $n \rightarrow \infty$, the claimed lower bound is obtained. \square

Theorem 3. $\liminf_{n \rightarrow \infty} \frac{1}{2n} \log Z_{2n}(\beta_m)$ is non-analytic at β_m^0 where $0 \leq \beta_m^0 \leq 2 \log \mu_3 - \log \mu_2$.

Proof: We can rewrite the result of theorem 2 as

$$\liminf_{n \rightarrow \infty} \frac{1}{2n} \log Z_{2n}(\beta_m) \geq \alpha \left[\frac{1}{2} (\log \mu_2 + \beta_m) - \log \mu_3 \right] + \log \mu_3$$

and this is equal to $\log \mu_3$ when

$$\frac{1}{2} (\log \mu_2 + \beta_m) - \log \mu_3 = 0, \quad \text{for } 0 < \alpha < 1.$$

This shows that the limiting infimum is greater than $\log \mu_3$ when $\beta_m > 2 \log \mu_3 - \log \mu_2$. Therefore the limiting infimum is singular at some β_m^0 where

$$0 \leq \beta_m^0 \leq 2 \log \mu_3 - \log \mu_2$$

which completes the proof. \square

3.1 Bounds on the free energies of linked conformations

The free energies of linked conformations of specified links can also be bounded using arguments similar to the above. We proceed by recalling that the growth constant of unknotted polygons is defined by the limit [5]

$$\lim_{n \rightarrow \infty} \frac{1}{n} \log p_n(\emptyset) = \log \mu_\emptyset. \quad (3)$$

It is known that $\mu_\emptyset < \mu_3$ [5, 6]. One may similarly define the growth constant μ_K of knotted polygons of knot type K by

$$\limsup_{n \rightarrow \infty} \frac{1}{n} \log p_n(K) = \log \mu_K. \quad (4)$$

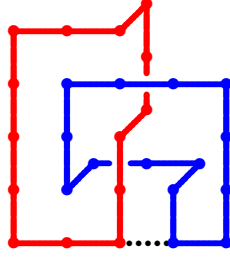


Figure 2: A linked conformation of two polygons with one mutual contact shown. The total number of mutual contacts between the two polygons is $k_m = 13$, while each polygon component has length $n = 14$. In this case the link type is $L = 2_1^2$, the Hopf link.

It is known that $\mu_\emptyset \leq \mu_K < \mu_3$ [7]

Denote the number of linked conformations of link type L , with polygon components of length n each, and with k_m mutual contacts, by $p_{2n}^{(2)}(k_m, L)$. The partition function is

$$Z_{2n}^{(2)}(\beta_m, L) = \sum_{k_m} p_{2n}^{(2)}(k_m, L) e^{\beta_m k_m} \quad (5)$$

and it is a sum of weighted conformations of fixed linked type L and total length $2n$.

An example of a linked conformation in our model is shown in figure 2. This conformation is a Hopf-link and it has weight $e^{13\beta_m}$ (since $k_m = 13$) in the partition function. More generally, the two components of a lattice link of link type L are lattice knots of knot types K_1 and K_2 respectively. In many cases $K_1 = K_2 = \emptyset$ (for example, if L is the Hopf link, as shown in figure 2), but K_1 and K_2 could be (necessarily) non-trivial knots for certain link types, or could be chosen to be given knot types.

We generalize theorem 1 as follows.

Theorem 4. *Suppose that L is a 2-component link with components of knot types K_1 and K_2 . Then, if $-\infty < \beta_m \leq 0$,*

$$\log \mu_\emptyset \leq \liminf_{n \rightarrow \infty} \frac{1}{2n} \log Z_{2n}^{(2)}(\beta_m, L) \leq \limsup_{n \rightarrow \infty} \frac{1}{2n} \log Z_{2n}^{(2)}(\beta_m, L) < \log \mu_3.$$

In the event that $K_1 = K_2 = \emptyset$, then $\lim_{n \rightarrow \infty} \frac{1}{2n} \log Z_{2n}^{(2)}(\beta_m, L) = \log \mu_\emptyset < \log \mu_3$.

Proof: An upper bound is obtained by first noting that $Z_{2n}^{(2)}(\beta_m, L) \leq Z_{2n}^{(2)}(0, L)$, and then counting the number of conformations of the component polygons independently, times the number of ways they may be placed so that the link may be recovered. Each component polygon is a placement of a simple closed polygon of fixed knot type, say K_1 for the first polygon, and K_2 for the second polygon. This shows that

$$Z_{2n}^{(2)}(1, L) \leq n^3 p_n(K_1) p_n(K_2)$$

Taking logarithms, dividing by $2n$ and letting $n \rightarrow \infty$, gives

$$\limsup_{n \rightarrow \infty} \frac{1}{2n} \log Z_{2n}^{(2)}(\beta_m, L) \leq \frac{1}{2}(\log \mu_{K_1} + \log \mu_{K_2}) < \log \mu_3.$$

In the event that the two component polygons of the link are both the unknot, then $K_1 = K_2 = \emptyset$ and

$$\limsup_{n \rightarrow \infty} \frac{1}{2n} \log Z_{2n}^{(2)}(\beta_m, L) \leq \log \mu_\emptyset.$$

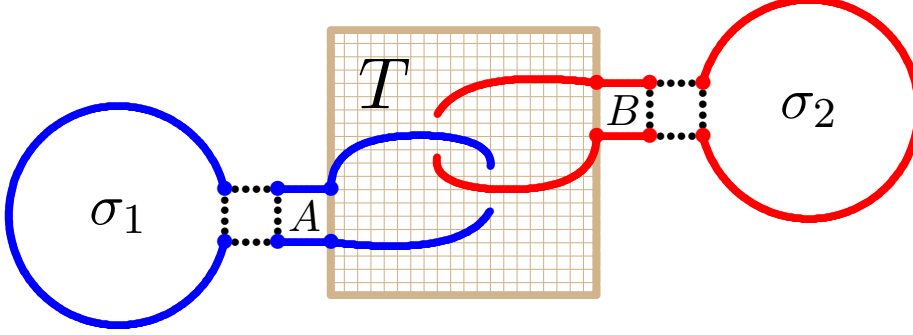


Figure 3: A schematic diagram with a construction to create a link in the cubic lattice. The link is represented by a tangle T drawn inside a square in the $x_3 = 0$ plane of the lattice. By subdividing the cubic lattice, the tangle can be pushed onto the edges in the $x_3 = 0$ plane and only stepping into the $x_3 = 1$ plane to create overpasses in the projection. Moreover, one component of the tangle has endpoints in the left-most boundary of the square while the other has endpoints in its right-most boundary. By adding edges at A and B respectively, the components of T can be closed into polygons such that the bottom and top edges of T are in different components. The top edge of an unknotted polygon σ_1 is concatenated to the bottom edge of T at A , and the bottom edge of an unknotted polygons σ_2 is concatenated to the top edge of T at B .

Consider the schematic diagram in figure 3 to find the lower bound. A link L is represented as a two-dimensional tangle T which is embedded in the $x_3 = 0$ plane of the cubic lattice, accommodating overpasses in T by stepping into the $x_3 = 1$ plane. The embedding of T is completed into a link by closing each component into a polygon such that the edge with lexicographic least midpoint (the *bottom edge*), and the edge with lexicographic most midpoint (the *top edge*), are in different components of the tangle. This is shown as A and B in figure 3.

Proceed by concatenating the top edge of an unknotted polygon σ_1 onto the bottom edge A , and the bottom edge of a second unknotted polygon σ_2 onto the top edge B , as illustrated. Assume that the length of the first component in the embedded tangle T is m_1 , and of the second component, m_2 . Fix the length of σ_1 to be $n - m_1$, and of σ_2 to be $n - m_2$. This creates a link L of link type determined by T , and since the overpasses in T are accommodated by overstepping into the $x_3 = 1$ plane, there is at least one mutual contact between the components of T , as required. There are $j_m \geq 1$ mutual contacts in L , and $j_m \leq 4(m_1 + m_2)$ since a polygon of length m_1 has at most 4 mutual contacts for each vertex, and since σ_1 and σ_2 do not contribute any such mutual contacts.

Since the orientation of the top edge of σ_1 has to match that of A , there are $p_{n-m_1}(\emptyset)/2$ choices for σ_1 . Similarly, there are $p_{n-m_2}(\emptyset)/2$ choices for σ_2 . This shows that

$$p_{n-m_1}(\emptyset) p_{n-m_2}(\emptyset) e^{\beta_m j_m} \leq 2^2 Z_{2n}^{(2)}(\beta_m, L).$$

Take logarithms, divide by $2n$, and let $n \rightarrow \infty$. Since m_1 and m_2 are fixed, this shows that

$$\log \mu_\emptyset \leq \liminf_{n \rightarrow \infty} \frac{1}{2n} \log Z_{2n}^{(2)}(\beta_m, L).$$

This completes the proof. \square

Lower bounds on the free energies of linked conformations of the model in figure 1(a) are determined using a construction similar to that in the proof of theorem 2. A schematic diagram is shown in figure 4. The intersection of the $x_3 = 0$ and $x_3 = 1$ planes and \mathbb{Z}^3 is a *slab* S of height 1. (That is, S consists of two square lattice planes a distance one apart in the x_3 -direction). Let T be a tangle diagram of a link of type L . Then T can be realised as two self-avoiding walks in S such that the endpoints of the self-avoiding walks are in a plane $x_1 = k$, and with the self-avoiding walks confined to the lattice points in S with $x_1 \leq k$. We next translate the tangle, and extend the endpoints of its component self-avoiding walks by adding steps, if necessary, into the $x_1 > k$ sublattice such that the two component self-avoiding walks have the same lengths ℓ , and the the four endpoints have coordinates $(m, 0, 0)$ $(m, 0, 1)$, $(m, 1, 0)$ and $(m, 1, 1)$ where $(m, 0, 0)$ and $(m, 1, 0)$ are the endpoints of one self-avoiding walk, and $(m, 0, 1)$ and $(m, 1, 1)$ are the endpoints of the second self-avoiding walk. By adding two edges to close off the tangle into a linked pair of polygons, the link L is realised as a lattice link of type L . We assume that there are c_0 mutual contacts between the component self-avoiding walks.

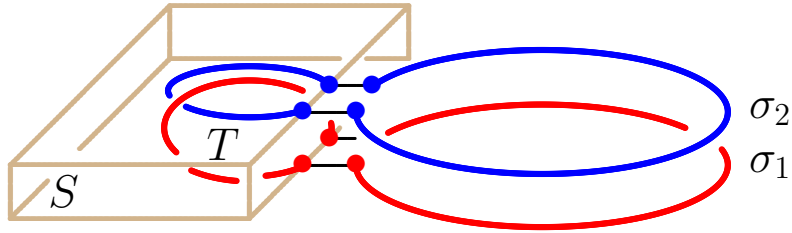


Figure 4: Schematic of a tangle T embedded in a slab S and two polygons σ_1 and σ_2 , each of length n , concatenated onto the components of the tangle. Since σ_2 is a translation of σ_1 one step along the x_3 -direction, the number of mutual contacts between them is n .

As shown in figure 4, let σ_1 be a square lattice self-avoiding polygon in the $x_3 = 0$ plane, and σ_2 be the translate of σ_1 one step in the x_3 -direction. If the length of σ_1 is n , then there are n mutual contacts between the pair of polygons (σ_1, σ_2) . This pair can be translated together and concatenated on the link L by placing the left-most and nearest edge (the bottom edge) of σ_1 one step in the x_1 -direction to the edge joining the endpoints $(m, 0, 0)$ and $(m, 1, 0)$. Then σ_2 has its bottom edge one step in the x_1 -direction from the edge joining the endpoints $(m, 0, 1)$ and $(m, 1, 1)$. The concatenation gives a lattice link of type L , with total length $2\ell + 2n + 2$. The total number of mutual contacts is $c_0 + n$. This shows that

$$Z_{2\ell+2n+2}^{(2)}(\beta_m, L) \geq q_n \beta_m^{c_0+n}, \quad (6)$$

since the number of choices for σ_1 is q_n , the number of square lattice polygons of length n .

By taking logarithms of equation (6), dividing by $2n$ and then taking $n \rightarrow \infty$, the following theorem is proven.

Theorem 5. *If $\beta_m > 0$ then $\liminf_{n \rightarrow \infty} \frac{1}{2n} \log Z_{2n}^{(2)}(\beta_m, L) \geq \frac{1}{2} (\log \mu_2 + \beta_m)$.* \square

The corollary of theorems 2 and 5 is that there is, for some link types, a critical point $\beta_m^{(L)}$.

Corollary 1. *Suppose that L is a link with components each of knot type the unknot. Then the limit $\liminf_{n \rightarrow \infty} \frac{1}{2n} \log Z_{2n}^{(2)}(\beta_m, L)$ is non-analytic at a critical point $\beta_m^{(L)}$, where $0 \leq \beta_m^{(L)} \leq 2 \log \mu_0 - \log \mu_2$.*

Proof: Note that if $\beta_m \leq 0$, then by theorem 4, $\lim_{n \rightarrow \infty} \frac{1}{2n} \log Z_{2n}^{(2)}(\beta_m, L) = \log \mu_\emptyset$. On the other hand, if $\beta_m > 0$, then by theorem 5, $\liminf_{n \rightarrow \infty} \frac{1}{2n} \log Z_{2n}^{(2)}(\beta_m, L) \geq \frac{1}{2}(\log \mu_2 + \beta_m)$. This lower bound is greater than $\log \mu_\emptyset$ if $\beta_m > 2 \log \mu_\emptyset - \log \mu_2$. Thus, there is a non-analyticity at a critical point $\beta_m^{(L)} \in [0, 2 \log \mu_\emptyset - \log \mu_2]$ in $\liminf_{n \rightarrow \infty} \frac{1}{2n} \log Z_{2n}^{(2)}(\beta_m, L)$ as claimed. \square

Since $\mu_\emptyset < \mu_3$ the upper bound in corollary 1 is strictly smaller than the upper bound given in theorem 3. In addition, note that the probability of seeing a link of type L (and with both components the unknot), is

$$P_{2n}(L) = \frac{Z_{2n}^{(2)}(\beta_m, L)}{Z_{2n}(\beta_m)}. \quad (7)$$

By theorems 1 and 4,

$$P_{2n}(L) = K \left(\frac{\mu_\emptyset}{\mu_3} (1 + o(1)) \right)^{2n} \rightarrow 0, \quad \text{if } n \rightarrow \infty \text{ and } \beta_m \leq 0. \quad (8)$$

Since $|\mu_3 - \mu_\emptyset| \approx 10^{-6}$ [8, 9], the convergence of $P_{2n}(L)$ to zero is numerically very slow and not significant until walks have lengths of $O(10^6)$, this effect will not be visible in our data, and the probability of linking as a particular fixed link type L will be a function of the local geometry of the polygons in the lattice and the value of β_m .

4 Results: Thermodynamic and metric properties

4.1 Monte Carlo method

Conformations of the lattice model were sampled from the Boltzmann distribution using a Markov chain Monte Carlo algorithm. The elementary moves were a combination of pivot moves for self-avoiding polygons [10] and local Verdier-Stockmayer style moves [11]. The Verdier-Stockmayer moves were introduced to increase the mobility of the Markov Chain when the algorithm samples at large positive values of β_m [12, 13] where there is a strong interaction between the component polygons which reduces the success rates of the pivot moves.

Sampling was also improved by implementing the elementary moves using a Multiple Markov Chain algorithm with chains distributed along a sequence of parameters $(\beta_m^{(j)})$ for $j = 1, 2, \dots, M$. Along each parallel chain Metropolis sampling was implemented to sample from the Boltzmann distribution at a fixed $\beta_m^{(j)}$, and chains were swapped using the protocols of Multiple Markov Chain sampling [14, 12, 13]. The collection of parallel multiple Markov chains is itself a Markov Chain with stationary distribution the product of the Boltzmann distributions along each chain (see reference [12, 13]).

In this paper we sampled along $M \approx 50$ parallel chains, and we were able to obtain sufficiently uncorrelated samples for systems of *total* size $2n \in \{96, 200, 296, 400, 600, 800\}$ and for the $\beta_m^{(j)}$ equally spaced in the interval $[-0.3, 1.0]$. We counted a single iteration as $O(1)$ pivot moves, and $O(n)$ local Verdier-Stockmayer style moves. By spacing the reading of data along each Markov chain, we were able to sample approximately 2.5×10^4 conformations that are essentially *uncorrelated* at each fixed value of $\beta_m^{(j)}$ for a total of at least 1.25×10^6 data points for each value of n . The simulations were expensive in terms of CPU time. For example, for $2n = 600$ and $M \approx 50$ a total of 25,000 uncorrelated conformations were sampled over three months of CPU time. In figure 6 we show some examples of conformations taken along the chains for different values of $\beta_m^{(j)}$.

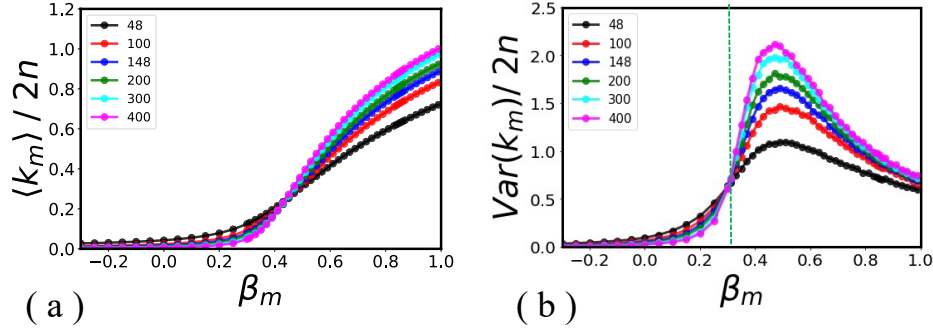


Figure 5: (a) Plot of the average number of mutual contacts per monomer, $\langle k_m \rangle / 2n$ and (b) the corresponding variance $Var(k_m) / 2n$ as a function of β_m . Different symbols refer to different values of n (see legend). In panel (b) the dashed vertical line highlights the location of the most asymptotic crossings that we consider as the best estimate of the transition

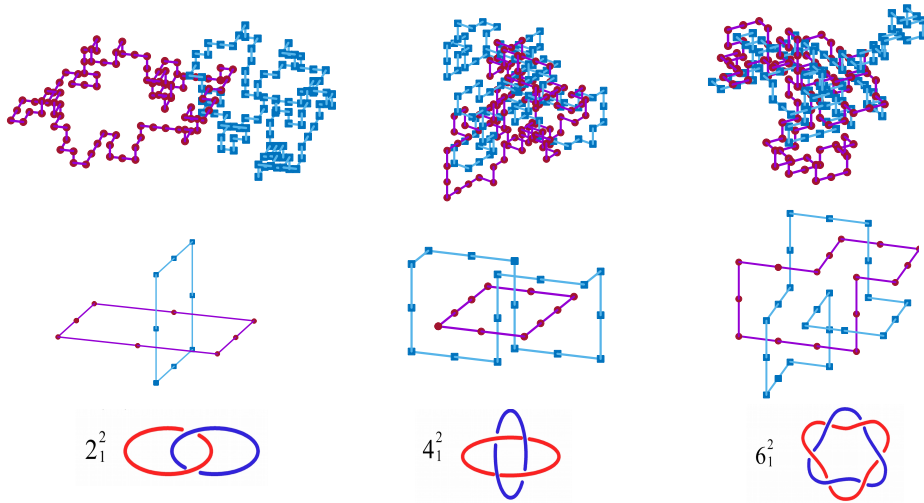


Figure 6: Top row: Pairs of lattice polygons, each of $n = 100$ steps sampled at different values of β_m 's (0.0, 0.4, 0.6). Their corresponding, topologically equivalent, simplified versions after the smoothing and shrinking procedure via the BFACF algorithm are reported in the middle row while the minimal representation of the associated link type is reported in the bottom row.

4.2 Thermodynamic properties

The results in section 2 show that there should be two regimes in the model, namely a segregated regime for negative or small positive values of β_m , and a mixed regime of interpenetrating components when β_m is large and positive. The segregated regime is characterized by states where the two polygons are separated from one another with a low density of mutual contacts between them, while the mixed phase has the two components close together in the same local space so that the number of mutual contacts is increased.

A sharp change in the average energy per monomer $\langle k_m \rangle / (2n)$ is consistent with the two regimes being separated by a phase boundary (see section 3). This is also seen in the variance of $\langle k_m \rangle$ defined by

$$Var(k_m) = \langle k_m^2 \rangle - \langle k_m \rangle^2. \quad (9)$$

Estimates of $\langle k_m \rangle / (2n)$ and the normalized variance $Var(k_m) / (2n)$ are plotted as functions of β_m for various values of n in figure 5(a) and in figure 5(b), respectively. For $\beta_m < \beta_m^*$, $\langle k_m \rangle / (2n)$, tends to zero with increasing n . In this phase the small and decreasing number of mutual contacts per monomer is consistent with the two component polygons being largely segregated in space. This is the *segregated phase*, as explained in section 3. For $\beta_m > \beta_m^*$ the curves of $\langle k_m \rangle / (2n)$ are increasing as n increases. In this *mixed phase* the two polygons have large non-zero energy per monomer (that is, a high incidence of mutual contacts), consistent with the two component polygons having sections near to each other in the lattice as they share the same volume in space. Our data are consistent with $\langle k_m \rangle \rightarrow An$ as n increases with $2 < A \leq 3$. This shows that the mixed phase is not an extended ribbon with the two polygons forming its boundary, but is a denser phase where strands in each polygon have a high number of contacts per monomer (between 2 and 3) with the other component. The segregated-mixed transition as β_m is taken through its critical value is also seen in the peak forming in $Var(k_m) / 2n$ when plotted as a function of β_m , see figure 5(b). With increasing n the peaks move to smaller values of $\beta_m^{(p)}$. This behaviour is consistent with theorems 1 and 2, since in the infinite n limit the variance is equal to zero in the segregated phase, has a jump discontinuity at the critical point, and then decreases with increasing β_m .

The data in figure 5(b) strongly suggest that the transition at β_m^* is asymmetric (that is, in the limit $n \rightarrow \infty$ the variance is zero if $\beta < \beta_m^*$ but it characteristically increases as $\beta \searrow \beta_m^*$). In these circumstances the intersections of the variances for different values of n in figure 5(b) are a good estimator of the location of the critical point as $n \rightarrow \infty$. This gives the estimate of $\beta_m^* = 0.31 \pm 0.01$. The asymmetry of the transition is consistent with the results of section 3.

4.3 Metric and shape properties

The size and metric scaling of lattice links can be examined by calculating metric quantities such as the mean square radius of gyration R_j^2 for $j \in \{1, 2\}$ for components $j = 1$ or $j = 2$. As expected the behaviour of R_j^2 does not depend on j and we improve the estimate of this metric observable by averaging over the two components: $R_g^2 = (R_1^2 + R_2^2) / 2$. This quantity, scaled by the power $n^{2\nu}$ is reported, as a function of β_m , in figure 7(a) and (b), and for lengths $n \in \{48, 100, 148, 200, 300, 400\}$. Since the metric scaling of the self-avoiding walk has exponent $\nu_{SAW} = 0.587297(7)$ [15] it should be the case that the ratio $R_g^2 / n^{2\nu_{SAW}}$ is a constant for $\beta_m < 0$ (in the segregated regime). This is seen in figure 7(a) where the data for $\beta \leq \beta_m^* \approx 0.3$ collapse to a constant close to 0.1, with little dependence on n . This is evidence that for these values of β_m the system is in a *segregated phase* where the self-avoidance between the two polygons separates them in space, and each polygon has the properties of a ring polymer in a good solvent, with associated metric exponent ν .

For values of $\beta_m > \beta_m^*$ the model is instead in a mixed phase. Here the ratio $R_g^2 / n^{2\nu}$ with $\nu = \nu_{SAW}$ is dependent on both n and β_m , decreasing either with increasing β_m or with increasing n , as seen in figure 7(a). The collapsed nature of the model is exposed by plotting $R_g^2 / n^{2/3}$ against β_m , showing collapse of the data for different values of n to an underlying curve for large values of β_m , see figure 7(b). These observations are consistent with the model passing through a phase transition into a mixed and *collapsed* phase where the interpenetrating components explore states with a high (local) density of monomers. Note that in this figure the critical point β_m^* separating the segregated and mixed phases has value approximately 0.3, that is, consistent with the one estimated using the variance of the mutual number of contact (see figure 5(b)).

The collapse of the data for large $\beta_m > \beta_m^*$ is consistent with the two polygons interpenetrating

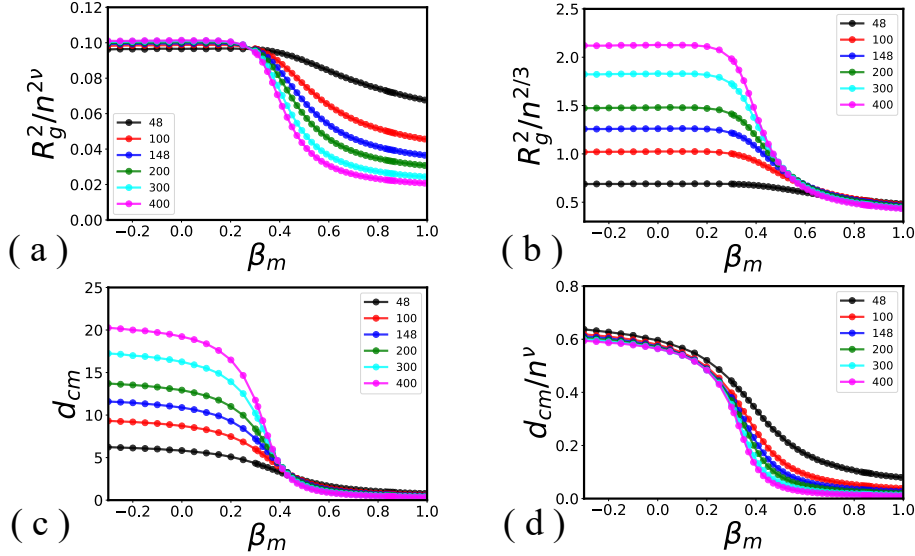


Figure 7: (a,b) $\langle R_g^2 \rangle / n^{2\nu}$ for $\nu = \nu_{SAW}$ (a) and $\nu = 1/3$ (b). (c) Average distance between the centres of mass of the two rings $\langle d_{cm} \rangle$ as a function of β_m . (d) Same as (c) but now scaled by n^ν with $\nu = \nu_{SAW}$. Different symbols refer to different values of n (see legend).

each other in a phase with high mutual contacts. This indicates that the mixed phase may be characterized by compact conformations in a collapsed phase and that the lattice link transitions through a θ -point at β_m^* from an expanded and segregated phase into a collapsed and mixed phase.

The transition between a segregated (and expanded or free) phase for negative β_m , and a mixed (and collapsed) phase for large positive β_m , is also suggested by other metric observables. For instance, in figure 7(c) and (d) the mean separations between the centres of mass d_{cm} of the two polygon components are examined. The β_m dependence of this measure is reported in figure 7(c) while in figure 7(d) the scaled version d_{cm}/n^ν is plotted. In both cases the data decrease with increasing β_m , consistent with the model entering a compact phase where the centres of mass of the two components are close to each other. Note that in (c) d_{cm} increases with n in the segregated phase, and this growth is shown in (d) to be at the expected rate of $O(n^\nu)$, the typical length scale of the model. The curves in (c) intersect pairwise close to a critical value $\beta_m^* \approx 0.4$, slightly larger than the estimate suggested by the data of figure 7(a), but not inconsistent with the expected segregated-mixed transition.

The configurational properties of the model change as it crosses over from the segregated phase to the mixed phase. The interaction between the two polygon components, due to both the self-avoidance repulsion, and the short ranged interaction induced by weighted mutual contacts, deform the components in the two phases, and this may be seen by measuring the asphericity and prolateness of components. In the segregated phase the conformations may be similar to that shown in figure 6 (left), while the mixed phase has interpenetrated components as shown in figure 6 (middle and right). In the segregated phase the polygon components are aspherical when the components are segregated, but transitioning into the mixed phase reduces the degree of asphericity as the two components collapse by forming mutual contacts and interpenetrate into a locally dense conformation. This is seen in figure 8(a) where the average asphericity $\Delta = (\Delta_1 + \Delta_2)/2$ is highest in the segregated phase but decreases once the model transitions through a critical value of β_m into the

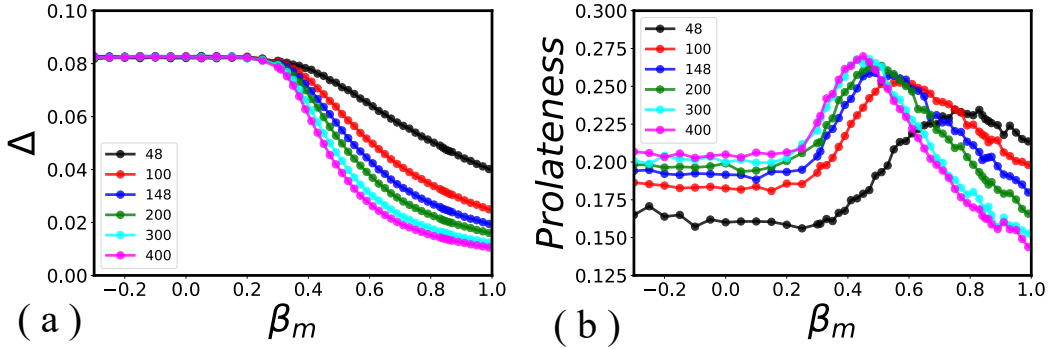


Figure 8: Asphericity Δ (a) and degree of prolateness (b) as a function of β_m . Note that the value of β_m at which Δ deviates from the constant value characterizing the segregated phase and the most asymptotic position of the peaks in the prolateness (i.e. $n = 400$) are consistent with the value of β_m^* .

mixed phase. In the segregated phase the data are collapsed into a horizontal line (independent of both β_m and n) with the asphericity $\Delta \approx 0.08$ over the entire range of the segregated phase). In the mixed phase Δ decreases with increasing β_m and increasing n .

The degree of prolateness of the model (plotted in figure 8(b)) presents a more nuanced picture, and our data are more noisy. They suggest a relatively constant (in β_m) value in the segregated phase that increases and appears to peak in the mixed phase at a location that moves to smaller values of β_m with increasing n approaching the expected value β_m^* . When $\beta_m \leq 0$ the main effect is entropic repulsion where the two curves are mutually repelling (for entropic reasons), leading to the two components being prolate. As β_m increases towards its critical value the two components will start to intermingle but there will still be parts of each component that are not intermingled (so that the components are not completely mixed). These intermingled parts might feel a stronger entropic repulsion resulting in a more prolate shape. For large β_m the mutual attraction dominates, and this will overcome the entropic repulsion and give a more spherical shape when the two components are mixed. Clearly, from the figure, this effect is small.

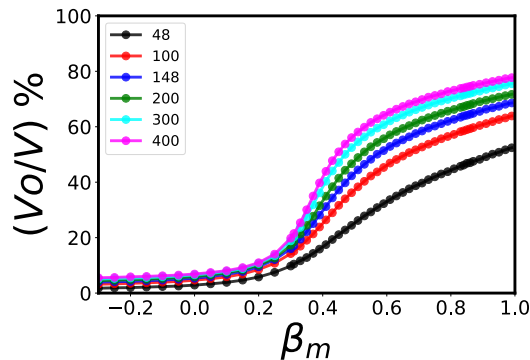


Figure 9: Percentage of the volume fraction of the region shared by both polygons as a function of β_m .

A natural observable for the segregated/mixed transition is based on the estimate of the overlap volume fraction, V_o/V , namely the volume of the box shared by the two polygons scaled by the total volume of the box containing the full system [16]. This is shown as a function of β_m in figure 9. If

$\beta_m < \beta_m^*$ the overlap is relatively small (although not zero) and its value increases very mildly with n . When $\beta_m > \beta_m^*$ the overlap volume fraction V_o/V steadily increases approaching an asymptotic value that for $n = 400$ approaches the 80% of the system volume. This indicates a very strong interpenetration of the two rings when the system is well inside the mixed phase ($\beta_m = 1$).

5 Topological entanglement

5.1 Linking probability and average linking number

A first characterization of the topological mutual entanglement that forms in the system is provided by the estimate of the probability that the two polygons are topologically linked. In general two disjoint simple closed curves C_1 and C_2 are topologically unlinked (or splittable) if there exists a homeomorphism H of \mathbb{R}^3 onto itself, $H : \mathbb{R}^3 \rightarrow \mathbb{R}^3$, such that the images $H(C_1)$ and $H(C_2)$ can be separated by a plane [17]. This definition is not convenient computationally and we relied instead on the notion of linking based on the computation of the 2-variable Alexander polynomial $\Delta(t, s)$ of the link diagram. This is done by encoding crossings (overpasses and underpasses in a planar projection of the polygon pair) and calculating $\Delta(t, s)$ from the encoding. For details see reference [17].

$\Delta(t, s)$ is not a perfect invariant able to distinguish all link types, but if we restrict ourselves to the identification of link types with minimal crossing number at most 7 its resolution will be sufficient for the analysis of the data. The calculation of $\Delta(t, s)$ could be prohibitively costly if the number of crossings n_c after a planar projection is very large. This occurs in particular when the two polygons are strongly overlapping in the mixed phase (that is, for β_m 's sufficiently large). The number of crossings was decreased by simplifying the polygons while keeping the topology unaltered using BFACF moves [18, 19] at low temperature [20, 21]. This reduces the system to components of close to minimal length compatible with the linked state. See figure 6 for some examples of simplified configurations. This implementation almost always reduced the number of crossings in the projections to well below 50, reducing the CPU time devoted to calculating $\Delta(t, s)$. Notice that if a component is reduced to length $n \leq 6$, then the pair cannot be linked for geometric reasons, so that a calculation of $\Delta(t, s)$ is not necessary.

The calculation of $\Delta(t, s)$ proceeded by performing 100 independent projections onto randomly oriented planes of the simplified configurations, then choose amongst these the projection P with the least number of crossings. $\Delta(t, s)$ is then calculated using P for $t, s \in \{2, 3\}$. This gives four values which are compared to the values computed from the explicit expression of $\Delta(t, s)$ for link types up to 7 crossings (see for instance [22]). Those cases where the Alexander polynomial is not trivial but does not correspond to a link with 7 or fewer mutual crossings in its minimal projection, are classified as *complex links*.

In figure 10(a) we show the probability P_{link} of topologically linked pairs of polygons (i.e. $\Delta(t, s) \neq 0$) as a function of β_m and for different values of n . There are clear qualitative trends seen in this graph and, in particular, P_{link} increases with β_m . For $\beta_m \lesssim 0.4$ P_{link} increases rapidly with β_m as the model transitions from the segregated into the mixed phase. At large values of β_m (well inside the mixed phase), P_{link} appears to settle on a value close to 0.9 at the larger values of n . We do not give data for $n = 300$ or $n = 400$ when $\beta_m \gtrsim 0.4$ because of a possibility of false positives for the unlink. There are link types with $\Delta(s, t) = 0$ but which are topologically linked. These link types start to appear in the standard knot table as having minimal crossing numbers

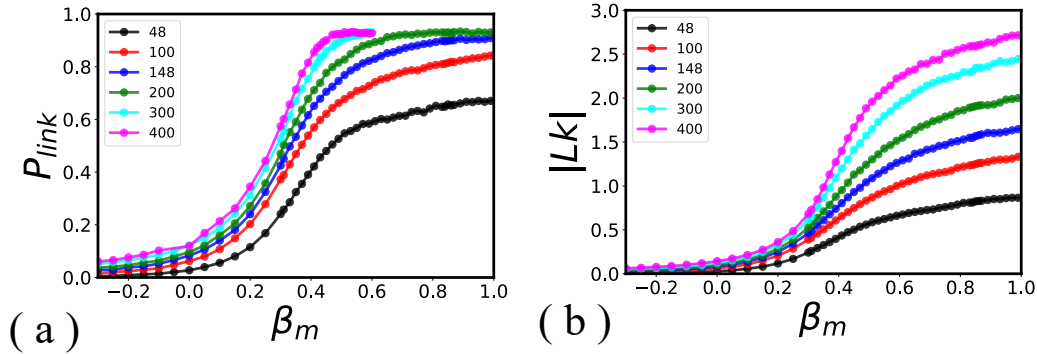


Figure 10: (a) Probability that a pair of polygons is linked as a function of β_m . (b) Average of the absolute value of the linking number as a function of β_m .

10. In our model as β_m increases the link types are of increasing complexity. Computing $\Delta(s, t)$ for some of these link types, however, gives $\Delta(s, t) = 0$, and they are classified as being the unlink. This causes overcounting of unlinks in our data at large n and high β_m , as well as undercounting of non-trivial links as a consequence. The result is that P_{link} would be systematically underestimated in figure 10(a) at large values of n and β_m .

A simpler way to measure the complexity of the linked states of the polygon pairs is by computing their linking number Lk . The linking number $Lk(C_1, C_2)$ of a pair of closed curves (C_1, C_2) is calculated by summing positive and negative mutual crossings in a simple projection of (C_1, C_2) [23]. The linking number defines homological linking of (C_1, C_2) , namely, two curves are homologically linked if and only if $Lk(C_1, C_2) \neq 0$ [17]. In figure 10(b) we report the average absolute value of $Lk(C_1, C_2)$, as a function of β_m . These graphs of $|Lk|$ increase for all values of β_m with n and with increasing β_m at fixed n . The increase is large in the mixed phase when $\beta_m > \beta_m^*$. It shows that both increasing n , and increasing β_m , increase the complexity of the links in the mixed phase, an effect which is much less pronounced in the segregated phase where the probability of linking is low.

5.2 Link spectrum

In figure 11 we examine aspects of the link spectrum measured as a function of β_m by plotting the percentage of the most popular links (with minimal crossing number up to 7 and with percentage at least 1%) as detected in our simulations. As expected, the population of unlinks is very large for $\beta_m < 0$ (approaching 100%), and decreases as β_m is increased and the mixed phase is approached.

For sufficiently large values of β_m and sufficiently large values of n , the proportion of unlinks stabilizes at very low levels. Concomitantly with this, the simplest link type (the Hopf link, 2_1^2) has a non-monotonic behaviour reaching a maximum at values of β_m that decrease as n increases. This non-monotonic behaviour is common to all link types with $n_c \leq 6$ and for the 7_1^2 and 7_2^2 links. The other 7 crossings links also show this behaviour but their populations are too small (below 1%) for this to be significant.

The fact that for large n and well inside the mixed phase the complexity of the linked pairs is rapidly increasing is also suggested by the rapid increase of the populations of topologically linked pairs ($\Delta(t, s) \neq 0$) having $n_c > 7$. This is reported in figure 12 together with two examples of

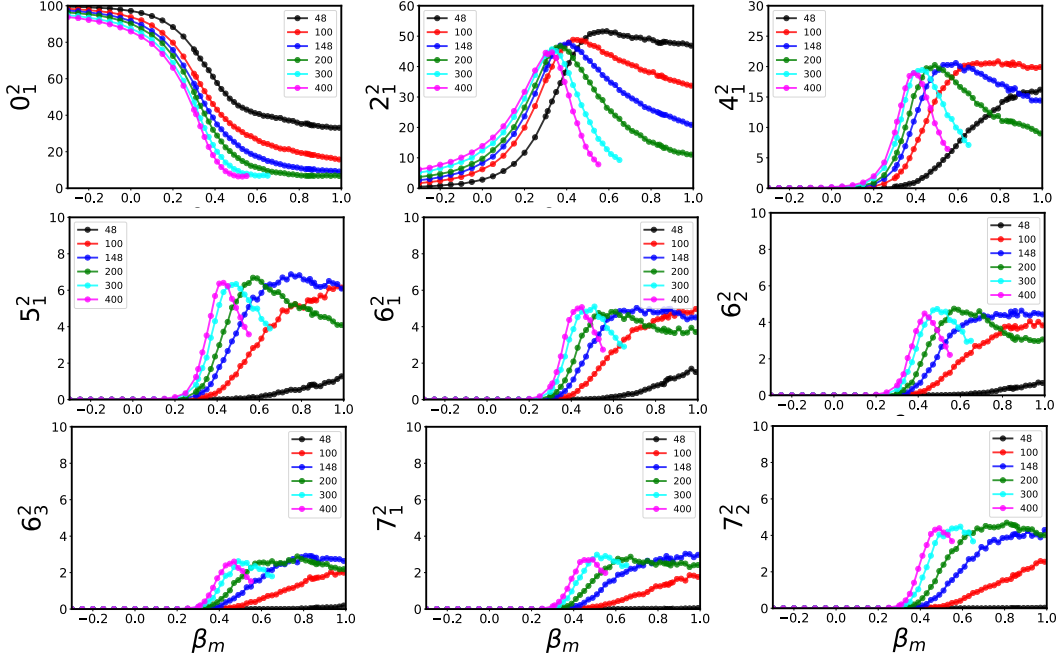


Figure 11: Percentage of the population of link types with $n_c \leq 6$ as a function of β_m for different values of n . The two link types 7_1^2 and 7_2^2 are the only two links with $n_c = 7$ whose relative populations are larger than 1%.

linked pairs of polygons with $n_c = 8$. Again, the fact that for $n \geq 300$ the curves seem to approach a constant value could be due to the failure of the two-variable Alexander polynomial in detecting more complex links at large β_m .

Finally, in figure 13 we report the link spectrum as a function of β_m where each panel presents data for a different value of n . In all cases the unlink dominates the segregated phase, but its incidence decreases sharply when $\beta_m \approx 0.3$ while the incidence of linked conformations increases into the mixed phase. The Hopf link (2_1^2) dominates the linked conformations in the mixed phase but it also peaks close to $\beta_m \approx 0.3$. More complex links also appear, albeit at smaller proportions, as β_m increases, and the simplest of these similarly peak at $\beta_m \approx 0.3$. It appears from our data that the number of link types multiplies in the mixed phase with increasing values of n , and while the incidence of specific link types decreases with increasing n and β_m , we know from figure 10 that the sum over all these link types increases with β_m into the mixed phase. This may indicate that the increase in the number of link types compensates for the reduction in the incidence of any specific link type, so that the proportion of linked conformations dominate state space.

5.3 Metric and energy properties at fixed link type

In figure 14 the number of mutual contacts in pairs of unlinked polygons is plotted as a fraction of the total number of mutual contacts. This fraction is (expectedly) close to one if β_m is negative, showing that almost all conformations are unlinked. Increasing β_m towards its critical value reduces this fraction, and this is consistent with both an increase in the total number of contacts due the components starting to approach one another, and with an increase in the proportion of linked conformations where the polygons are closer together and so contain larger numbers of mutual

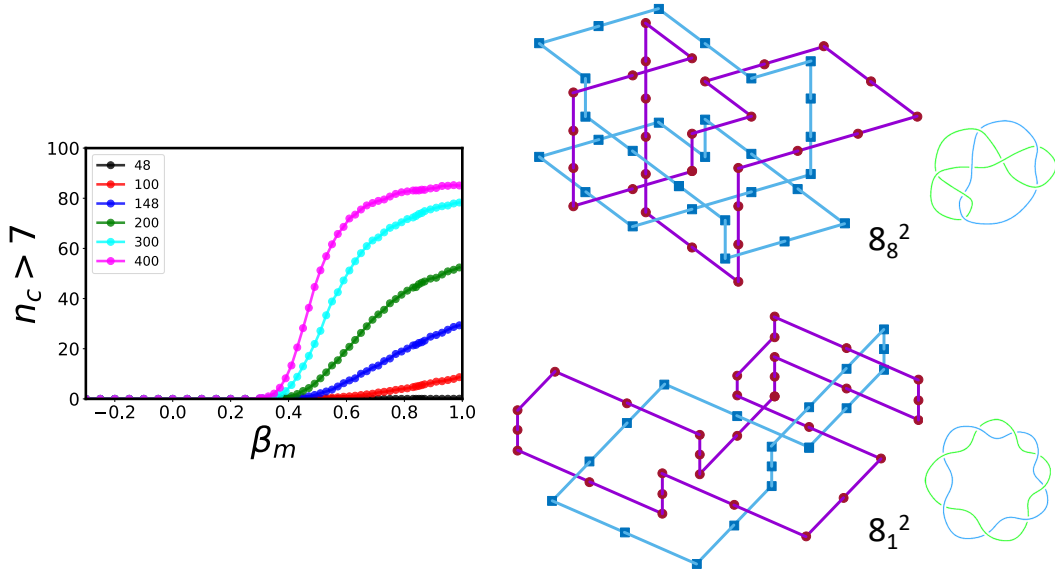


Figure 12: Percentage of the population of link types having $\Delta(t, s) \neq 0$ with $n_c > 7$. To give a glimpse of the complexity of the links found in the mixed state two examples with $n_c = 8$ are reported. The top right refers to a 8_8^2 link (Lk=1) and was found in a polygon pair with $n = 48$ while the bottom right is a 8_1^2 link (Lk=4) and was found in a polygon pair with $n = 100$. In both cases the configurations reported are those simplified by the smoothing algorithm based on BFACF moves, see text.

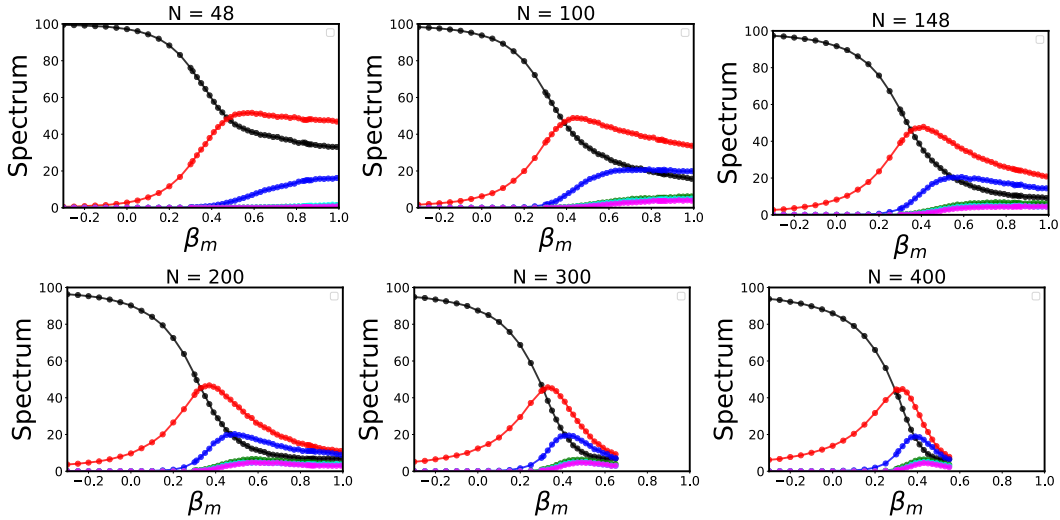


Figure 13: Percentage of the population of some link types as a function of β_m (black: 0_1^2 , red: 2_1^2 , blue: 4_1^2 , green: 5_1^2 , cyan: 6_1^2 , magenta: 6_2^2). Different panels refer to different values of n .

contacts. This observation is supported by noting that the ratio of contacts between links of type 2_1^2 and all polygons in the first instance, and between 2_1^2 and unlinked states are high in the segregated phase, showing that linked states of type 2_1^2 contain, on average, a higher density of mutual contacts.

Data on the mean square radius of gyration paint an interesting picture. Deep in the segregated

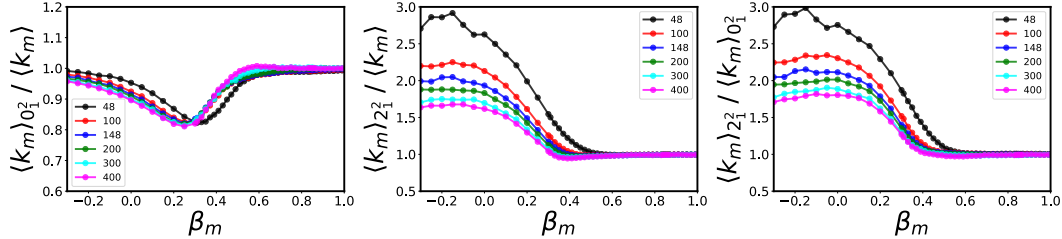


Figure 14: β_m dependence of the ratio between the energy of pairs of polygons with a given link type and the one for the set of all pairs of polygons or the set of a different link type.

phase the unlink dominates state space and so the ratio of $\langle R_g^2 \rangle_{0_1^2}$ to $\langle R_g^2 \rangle$ is approximately equal to 1. This is also the case deep in the mixed phase – unlinked states have about the same size as the average conformation (since the polygons are mixed and together collapsed into a dense conformation minimizing the $\langle R_g^2 \rangle$). Near the critical point the situation is more interesting. As the proportion of linked states increases as β_m approaches its critical value from below, the ratio $\langle R_g^2 \rangle_{0_1^2} / \langle R_g^2 \rangle$ increases because linked states are smaller than unlinked states. This ratio should exceed 1 (which it does). Passing through the transition causes collapse of both unlinked and linked states, and so the ratio should settle down to 1 again, as it does. This picture is reaffirmed in the figures plotting the ratios $\langle R_g^2 \rangle_{2_1^2} / \langle R_g^2 \rangle$ and $\langle R_g^2 \rangle_{2_1^2} / \langle R_g^2 \rangle_{0_1^2}$ showing that the link 2_1^2 is larger than the unlink and the average of all states in the segregated phase, but are about the same size in the mixed (collapsed) phase.

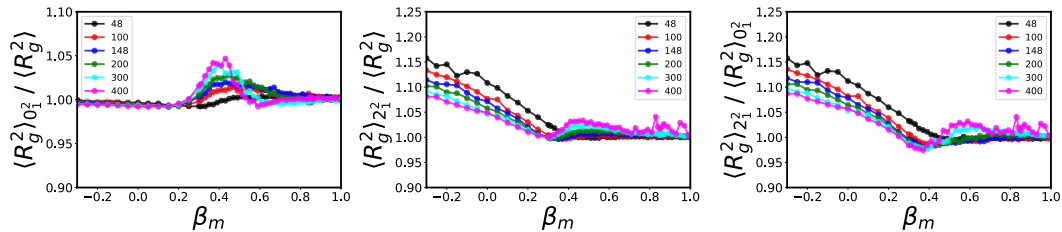


Figure 15: β_m dependence of the ratio between the mean-squared radius of gyration of polygons of a given link type and the value for all pairs of polygons or for pairs of a different link type.

6 Discussion

To investigate the thermodynamics, metric and topological properties of a pair of polymer rings undergoing a segregated to mixed phase transition, we have considered a pair of polygons on the simple cubic lattice constrained to have a pair of vertices (one from each polygon) unit distance apart. The polygons are self- and mutually avoiding and, in addition, there is a short range potential between pairs of vertices in the two polygons. When this potential is repulsive or weakly attractive the two polygons are largely separated in space but when the potential is sufficiently attractive the polygons interpenetrate and form a more compact object in a mixed phase.

In section 3 we prove that the limiting free energy exists when the potential is repulsive, and we establish bounds when it is attractive that establish the existence of a phase transition from a segregated phase to one where there are many inter-polygon contacts. We use a Monte Carlo

approach to investigate configurational properties such as the expected number of inter-polygon contacts, and the radius of gyration of a polygon as a function of the strength of the potential. The mean number of contacts increases as the potential becomes more attractive and increases rapidly in the region of the transition. The radius of gyration scales differently (with size) in the segregated and compact phases and there are changes in the asphericity and prolateness.

In section 5 we looked at the extent of linking of the two polygons as a function of the strength of the potential, both by computing the 2-variable Alexander polynomial (as a detector of topological linking) and the linking number (as a detector of homological linking). As the potential becomes more attractive the linking probability and the link complexity both increase, with a relatively sharp increase around the transition region. It is clear that, in the compact phase where there is considerable interpenetration of the polygons, the linking probability is high.

A related experimental situation is as follows. Consider a uniform 4-star polymer with two A -arms and two B -arms with the ends of the arms functionalized so that the system can be cyclized to form an A ring and a B ring, forming a figure eight. The A and B arms carry opposite charges so that they are attracted to one another and the strength of the attraction can be modified by changing the pH or the ionic strength. Prepare the system (ie the 4-star) at some fixed pH and ionic strength and, after equilibration, carry out a cyclization reaction. At high ionic strength or where charges are suppressed by varying the pH, the A and B arms will repel or weakly attract and there should be little interpenetration so that, after cyclization, there should be little linking. Conversely, with large charge densities and low ionic strength there should be considerable interpenetration and linking.

Acknowledgement

EJJvR acknowledges financial support from NSERC (Canada) in the form of a Discovery Grant RGPIN-2019-06303. Data generated for this study are available on reasonable request.

References

- [1] de Gennes P G 1979 Scaling concepts in Polymer Physics (Cornell University Press, Ithaca, New York)
- [2] Janse van Rensburg E J, Orlandini E, Sumners D W, Tesi M C and Whittington S G 1994 Phys. Rev. E **50** R4279
- [3] Janse van Rensburg E J, Orlandini E, Sumners D W, Tesi M C and Whittington S G 1996 J. Stat. Phys. **85** 103–130
- [4] Hammersley J M 1961 Math. Proc. Camb. Phil. Soc. **57** 516–523
- [5] Pippenger N 1989 Discr. Appl. Math. **25** 273–278
- [6] Sumners D W and Whittington S G 1988 J. Phys. A: Math. Gen. **21** 1689–1694
- [7] Soteris C E, Sumners D W and Whittington S G 1992 Math. Proc. Camb. Phil. Soc. **111** 75–91

- [8] Janse van Rensburg E J 2002 Contemporary Mathematics **304** 125–136
- [9] Baiesi M, Orlandini E and Stella A L 2010 J. Stat. Mech.: Theo. Exp. **2010** P06012
- [10] Madras N, Orlitsky A and Shepp L A 1990 J.Stat. Phys. **58** 159–183
- [11] Verdier P H and Stockmayer W H 1962 J. Chem. Phys. **36** 227–235
- [12] Tesi M C, Janse van Rensburg E J, Orlandini E and Whittington S G 1996 J. Stat. Phys. **82** 155–181
- [13] Tesi M C, Janse van Rensburg E J, Orlandini E and Whittington S G 1996 J. Phys. A: Math. Gen. **29** 2451
- [14] Geyer C J 1991 Comp. Sci. and Stat.: Proc. 23rd Symp. on the Interface 156–163
- [15] Clisby N 2010 Phys. Rev. Lett. **104** 055702
- [16] Orlandini E, Tesi M C and Whittington S G 2021 J. Phys. A: Math. Theo. **54** 505002
- [17] Rolfsen D 1976 Knots and Links (Mathematics Lecture Series 7, Publish or Perish, Inc., Houston, Texas)
- [18] Berg B and Foerster D 1981 Phys. Lett. B **106** 323–326
- [19] Aragao De Carvalho C and Caracciolo S 1983 J. de Physique **44** 323–331
- [20] Janse van Rensburg E J and Whittington S G 1991 J. Phys. A: Math. Gen. **24** 5553
- [21] Baiesi M, Orlandini E and Stella A L 2014 Macromol. **47** 8466–8476
- [22] The knot atlas http://katlas.org/wiki/Main_Page
- [23] Adams C C 1994 The Knot Book (Freeman)